Structure and Mechanism of the Influenza A M2$_{18-60}$ Dimer of Dimers

Loren B. Andreas[†], **Marcel Reese**[†], **Matthew T. Eddy**[†], **Vladimir Gelev**[‡], **Qing Zhe Ni**[†], **Eric A. Miller**[†], **Lyndon Emsley**[∥], **Guido Pintacuda**[§], **James J. Chou**[⊥], and **Robert G. Griffin**[*,†]

[†]Department of Chemistry and Francis Bitter Magnet Laboratory, Massachusetts Institute of Technology, 77 Massachusetts Avenue, Cambridge, Massachusetts 02139, United States [‡]Department of Chemistry and Pharmacy, Sofia University, 1 James Bourchier Boulevard, 1164 Sofia, Bulgaria [§]CNRS/ENS Lyon/UCB-Lyon 1, Université de Lyon, Centre RMN à Très Hauts Champs, 5 rue de la Doua, 69100 Villeurbanne, France [∥]Institut des Sciences et Ingénierie Chimiques, Ecole Polytechnique Fédérale de Lausanne (EPFL), 1015 Lausanne, Switzerland [⊥]Department of Biological Chemistry and Molecular Pharmacology, Harvard Medical School, Boston, Massachusetts 02115, United States

Abstract

We report a magic angle spinning (MAS) NMR structure of the drug-resistant S31N mutation of M2$_{18-60}$ from Influenza A. The protein was dispersed in diphytanoyl-*sn*-glycero-3-phosphocholine lipid bilayers, and the spectra and an extensive set of constraints indicate that M2$_{18-60}$ consists of a dimer of dimers. In particular, ~280 structural constraints were obtained using dipole recoupling experiments that yielded well-resolved $^{13}C-^{15}N$, $^{13}C-^{13}C$, and $^1H-^{15}N$ 2D, 3D, and 4D MAS spectra, all of which show cross-peak doubling. Interhelical distances were measured using mixed $^{15}N/^{13}C$ labeling and with deuterated protein, MAS at $\omega_r/2\pi = 60$ kHz, $\omega_{0H}/2\pi = 1000$ MHz, and ^1H detection of methyl–methyl contacts. The experiments reveal a compact structure consisting of a tetramer composed of four transmembrane helices, in which two opposing helices are displaced and rotated in the direction of the membrane normal relative to a four-fold symmetric arrangement, yielding a two-fold symmetric structure. Side chain conformations of the important gating and pH-sensing residues W41 and H37 are found to differ markedly from four-fold symmetry. The rmsd of the structure is 0.7 Å for backbone heavy atoms and 1.1 Å for all heavy atoms. This two-fold symmetric structure is different from all of the previous structures of M2, many of which were determined in detergent and/or with shorter constructs that are not fully active. The structure has implications for the mechanism of H$^+$ transport since the distance between His and Trp residues on different helices is found to be short. The structure also exhibits two-fold symmetry in the vicinity of the binding site of adamantyl inhibitors, and steric constraints may explain the mechanism of the drug-resistant S31N mutation.

Graphical abstract
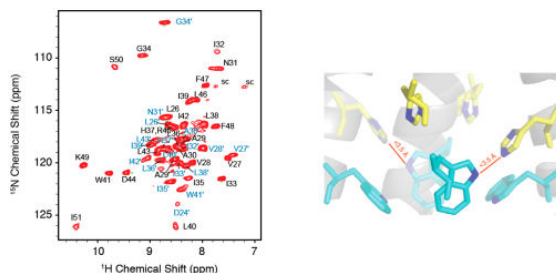
INTRODUCTION

Influenza A M2 is a 97 residue transmembrane protein that assembles as a tetramer[1] and conducts protons at low pH[2] in order to trigger membrane fusion in an endosome and unpacking of the viral genome.[3,4] The N-terminus of the protein is positioned on the outside of infected cells, with at least the first 18 residues exposed.[5,6] A single-pass α-helix places the C-terminal domain on the cytoplasmic side of infected cells, a portion of which forms an amphipathic helix responsible for stabilization of the protein.[7]

The M2 H^+ transporter is critical for viral replication, as evidenced by the therapeutic effect of aminoadamantyl inhibitors known to target M2 and to reduce proton conduction.[7] There are now several excellent structures of the wild-type (WT) protein in complex with aminoadamantyl inhibitors in the pore, placing the site of pharmacological binding between residues 27 and 34.[8–12] However, resistance has developed in circulating strains of influenza, primarily due to a single-point mutation S31N, which has precipitated a need for new inhibitors that target S31N M2. Since the proton conduction process in M2 is very sensitive to the structure of the peptide, this motivates the determination here of the structure of S31N M2 in hydrated lipid bilayers.

Previous structural studies of M2 have been applied to several different constructs reconstituted in a variety of virus membrane mimetics. These constructs can be classified into three groups, the full-length protein (FL), the conduction domain (CD), and the transmembrane domain (TM). The CD comprises approximately residues 18–60, which includes both the transmembrane residues (25–46) as well as an amphipathic helix (~47–59), which is known to stabilize the tetrameric assembly.[7,13] TM domain constructs from residue 22 to 46 contain a single membrane-spanning helix that does not fully reproduce the conduction and drug inhibition of WT but remains drug-sensitive. Since the CD forms tetramers with conduction and drug sensitivity that are indistinguishable from that of the full protein, we have investigated a CD construct, M2$_{18–60}$.[13]

Within the core of the tetrameric bundle, the four His-H37 residues are known to control the pH-dependent rate of conduction. Measurements on M2$_{22–46}$[14,15] and M2$_{18–60}$[16] showed a multiplicity of H37 pK_a values and pinpointed the third protonation event as being responsible for physiological conduction. Thus, although the channel is a homotetramer, H37 exists as a mix of imidazole and imidazolium,[17] implying that the highest degree of

symmetry for doubly protonated M2 tetramers is two-fold. In lipid bilayers, we find that two-fold symmetry is detected even for $M2_{18-60}$ tetramers that are uncharged at H37.[18–20]

Magic angle spinning (MAS), oriented sample (OS), and solution NMR have been used extensively to study various constructs of M2. The initial solid-state experiments were published by Cross and co-workers,[21–24] and more recently, Hong and co-workers[11,12,14,25] have made important contributions to the study of constructs of M2. Extensive solution NMR studies have been described by the groups of Chou[9,13,26] and DeGrado.[27–30]

Here we report MAS NMR studies of the $M2_{18-60}$ construct carrying the drug-resistant mutation S31N from Influenza A dispersed in diphytanoyl-*sn*-glycero-3-phosphocholine lipid bilayers. We employed a number of dipole recoupling experiments that yielded well-resolved $^{13}C-^{15}N$ and $^{13}C-^{13}C$ 2D and 3D MAS spectra that permit determination of structural constraints for membrane protein samples. Samples were isotopically labeled with several different schemes, including uniform ^{13}C and ^{15}N labeling, labeling by residue type, and site-specific ^{13}C labeling using 1,6-^{13}C glucose. Interhelical distances were measured unambiguously using mixed $^{15}N/^{13}C$ labeling. Several additional restraints were determined using extensively deuterated protein, MAS at $\omega_r/2\pi = 60$ kHz and $\omega_{0H}/2\pi = 1000$ MHz, and ^{1}H detection of methyl–methyl contacts in 3D and 4D MAS experiments. A mechanistically important $^{15}N-^{1}H-^{15}N$ distance of <3.5 Å was observed between His and Trp on the two different chains of the dimer. The experimental protocol could represent a paradigm for structural determinations of membrane protein samples. Collectively, these experiments yielded 283 structural constraints and permitted us to calculate a structure consisting of four compact transmembrane helices. However, importantly, two opposing helices are displaced and rotated in the direction of the membrane normal, yielding a two-fold symmetric structure. Side chain conformations of the important gating and pH-sensing residues W41 and H37 are found to differ markedly from four-fold symmetry. The rmsd of the structure is 0.7 Å for backbone and 1.1 Å for all heavy atoms. This two-fold symmetric structure is clearly different from all of the previously reported structures of WT M2 and from the two previously reported structures of S31N M2,[26,29] which were solved in detergent micelles.

The dimer of dimers structure reported here was determined in lipid bilayers that closely mimic the viral environment. We used a preparation that allowed pharmacological drug binding in WT M2,[8] supporting the assertion that we have reconstituted a native state of the protein. The structure calculated from the MAS NMR constraints therefore has implications for the path of H^+ transportation and inhibitor binding. In particular, there is direct contact between a His and Trp on different helices, which is likely important in H^+ transport. Furthermore, constriction within the tetramer at residues H37 and W41 excludes passage of water, consistent with the current understanding that M2 conducts via H^+ shuttling. Finally, the structure also exhibits two-fold symmetry in the vicinity of the site of adamantyl inhibitors, and comparison of steric constraints with drug-bound structures may explain the mechanism of the drug-resistant S31N mutation.

EXPERIMENTAL SECTION

M2 Synthesis

Recombinant M2 was synthesized, purified, and refolded in 1,2-diphytanoyl-*sn*-glycero-3-phosphocholine (DPhPC) bilayers at a lipid/protein ratio of 1:1 by weight as described previously.[18] Briefly, overexpression was carried out in *Escherichia coli* BL21 DE3[13,18] in minimal media prepared per liter with 3–4 g of glucose, 1 g of ammonium chloride, standard salts, and Centrum adult vitamins (1.5 mL of 2 pills in 40 mL, dissolved with shaking for 30 min). The construct used was an N-terminal fusion to TrpLE, with a His-9 tag. After nickel affinity purification under denaturing conditions of 6 M guanidine, the fusion was precipitated by dialysis against water. The fusion was cleaved in 70% formic acid using cyanogen bromide (1–3h at ~20 °C), diluted, and lyophilized. The resulting powder was dissolved in 2:1:1 formic acid/HFIP/water and injected onto a C4 column equilibrated at 5% isopropyl alcohol. The protein eluted near the end of a gradient from 5% isopropyl alcohol to 58:37:5 acetonitrile/2-propanol/water. All reverse-phase chromatography solutions had 0.1% trifluoroacetic acid. The pure protein was lyophilized. Lyophilized protein was refolded by dissolving the protein in octyl glucoside detergent solution, mixing with a lipid solution dissolved in minimal octyl glucoside, and removal of detergent by dialysis at ~20 °C against sample buffer (40 mM phosphate, 30 mM glutamate, 3 mM sodium azide, pH 7.8). For samples with mixed labeling, cells containing the differently labeled protein were mixed and purified together for convenience.

Deuterated and ILV methyl-labeled protein was produced as described below and reconstituted in $^2H_{78}$ DPhPC. $^2H_{78}$ DPhPC was synthesized in collaboration with FBReagents (Cambridge, MA). Details are provided in the Supporting Information.

U-^{13}C,^{15}N M2—Per liter, 3 g of ^{13}C glucose and 1 g of ^{15}N ammonium chloride (CIL), with another 0.5–1 g of ^{13}C glucose added at induction (150 μM IPTG, 18 °C), were added at an OD_{600} of 0.7–0.9. The final OD_{600} reached 3.5–4 after 18 h of expression at 18 °C and yielded up to 15 mg of pure protein.

U-^{13}C,^{15}N-[^{12}C,^{14}N-ILFY] M2—Per liter, 3 g of ^{13}C glucose and 1 g of ^{15}N ammonium chloride (CIL), with another 0.5–1 g of ^{13}C glucose, were added at induction. Cells were grown in 700 mL of media, with 300 mL of media used to dissolve the amino acids. When the OD_{600} reached 0.7, the reserved 300 mL of media was added, along with amino acids at natural isotopic abundance:[31,32] 150 mg of isoleucine, 150 mg of leucine, 50 mg of phenylalanine, and 100 mg of tyrosine (Sigma-Aldrich). Expression of protein was induced with 150 μM IPTG at 18 °C as before. The final OD_{600} reached 3.5–4.6 after 18 h of expression at 18 °C and yielded up to 15 mg of pure protein.

[1-^{13}C]Glucose-, [1,6-^{13}C$_2$]Glucose M2—Preparation was identical to that for U-^{13}C-^{15}N M2 except that specifically isotopically labeled glucose was used. The labeling pattern resulting from [1,6-^{13}C]glucose is the same as that from [1-^{13}C]glucose[33] (Omicron Biochemicals) except that the [1,6-^{13}C]glucose results in double the labeling level per site.

U-^{13}C,^{15}N,^{2}H-[^{12}C,^{13}C^{2}H$_2$^{1}Hδ1-Ile, ^{12}C,^{13}Cα,^{13}C′,^{13}C^{2}H$_2$^{1}Hδ2-Leu, ^{12}C,^{13}C^{2}H$_2$ ^{1}Hγ2-Val] M2—An overnight culture in 50 mL of 90% ^{2}H M9, 10% SOC media, was grown from a fresh transformation in BL21-DE3 until reaching an OD$_{600}$ of 2–3. Cells were then pelleted by centrifugation and transferred to 1 L of ^{2}H M9 media containing 3 g of ^{2}H–^{13}C glucose, 1 g of ^{15}N ammonium chloride, salts, and Centrum as before, in 1 L of 99.8% ^{2}H D$_2$O. The doubling time was 2 h. At an OD$_{600}$ of 0.65–0.75, ILV precursors were added: 75 mg of α-ketobutyric acid,[34] sodium salt 4-^{13}C 99%, 3,3,4,4-^{2}H$_4$, 98% (CIL), and 350 mg of 2-(^{13}C,^{2}H$_2$)methyl-4-(^{2}H$_3$)-acetolactate prepared as described previously.[35] Cells were harvested after 24–36 h and yielded up to 5 mg of pure protein. This labeling pattern results in methyl groups with isolated ^{13}C^{1}H spin pairs in an otherwise ^{2}H,^{12}C background at nearby sites. The protein was purified and refolded in ^{1}H buffers, resulting in complete exchange to ^{1}H at exchangeable sites such as the backbone amides.

U-^{13}C,^{15}N,^{2}H-[^{13}CH$_3$δ1-Ile] M2—The same protocol as above was used, but the precursor was 75 mg of ^{13}C4, 98%, 3,3-^{2}H$_2$, 98% α-ketobytryic acid, and sodium salt.

U-^{13}C,^{15}N,^{2}H-[^{13}C^{2}H$_2$^{1}Hδ2-Leu, ^{13}C^{2}H$_2$^{1}Hγ2-Val] M2—The same protocol as above was used, but the precursor was 350 mg of U-^{13}C,2-(^{2}H$_2$)methyl-4-(^{2}H$_3$)-acetolactate.

NMR Spectroscopy

NMR spectra were recorded on several high-field Bruker (Bruker Biospin, Billerica, MA) spectrometers operating at a ^{1}H frequency of 800, 900, and 1000 MHz, and using 3.2 mm E-free probes at 800 and 900 MHz and 1.3 mm probes at 800 and 1000 MHz. Spectra were also recorded using a home-built spectrometer designed by Dave Ruben and operating at a ^{1}H frequency of 750 MHz equipped with a Bruker 3.2 mm E-free probe. ^{13}C-detected spectra were recorded with 3.2 mm Bruker E-free probes, and ^{1}H-detected spectra were recorded with Bruker 1.3 mm solenoid probes tuned to HCN or HCD. The sample temperature was maintained at 20–30 °C using Bruker cooling units (BCU II or BCU extreme) or on the 750 MHz instrument, a Kinetics Thermal System XR air-jet system (Stone Ridge, NY). Chemical shifts are reported on the DSS scale using adamantane as a secondary reference.

Spectral Assignments

The first task in any NMR structural determination involves assigning the spectra. In the case of the dimer of dimers of M2$_{18–60}$, sequence-specific chemical shift assignments of ^{13}C and ^{15}N were determined from 3D ^{15}N–^{13}C–^{13}C correlations and 2D ^{13}C–^{13}C correlations. Assignment of amide ^{1}H and backbone ^{13}C and ^{15}N resonances was made independently using a suite of six ^{1}H-detected spectra and automated analysis via MATCH,[36] as recently reported.[37] These backbone resonance assignments were in agreement with those made manually using ^{13}C detection. Stereospecific methyl protons were assigned using ^{13}C–^{1}H and ^{13}C–^{13}C–^{1}H correlations and the known ^{13}C shifts. Since many of the approaches we employed are new to MAS experiments, the spectra we used for assignment are detailed below.

NCACX and NCOCX connectivity was determined using 2D ^{15}N–^{13}C ZF-TEDOR[38] and 3D ^{15}N–^{13}C–^{13}C TEDOR-RFDR[18,39–41] spectra recorded on U-^{13}C,^{15}N M2 and U-^{13}C,^{15}N-[^{12}C,^{14}N-ILFY] M2 as described previously.[18] Spectra were recorded at a field of 900 MHz (^1H) and 20 kHz spinning, using 83 kHz RFDR pulses, ~100 kHz ^1H decoupling during RFDR mixing, and 83 kHz decoupling during acquisition. Mixing periods for ZF-TEDOR and RFDR of 1.2 and 4.8 ms were used with XY-4 and XY-16 or XY-32 phase cycling for TEDOR and RFDR, respectively. The N–^{13}Ca plane from the TEDOR is shown in Figure 1, and selected strips from the 3D are shown in Figure 2. In Figure 1, we have differentiated the two sets of cross-peaks corresponding to the two members of the dimer with blue and black labels. The cross-peak doubling is particularly obvious for G34 and P25 and also for the important residues H37 and W41. The spectra of Figure 2 illustrate our ability to make consecutive assignments, as shown from P25 to A29. In all, two continuous stretches of backbone assignments were made from these spectra, one for each set of peaks from D24 to D44 and from P25 to Y52. A high magnetic field of 21 T was instrumental in obtaining such well-resolved spectra for assignment.

In Figure 3, we illustrate a 2D HN spectrum recorded using a ^1H–^{15}N CP transfer with $\omega_1/2\pi = 50$ kHz and ~4–10 kHz on the ^{15}N and ^1H channels, respectively. In addition, we extended this experiment to 3D with an (H)C$_a$NH spectrum[37,42] recorded using a H–C$_a$ CP with $\omega_1/2\pi = 35$–50 kHz ramp on ^1H and 10 kHz on ^{13}C, C$_a$-N CP with $\omega_1/2\pi = 35$ kHz and 25 kHz on C$_a$ and ^{15}N, with a 10% ramp, and N–H CP with $\omega_1/2\pi = 50$ kHz on ^{15}N and 4–10 kHz on ^1H. Selected strips from the spectrum are shown in Figure 4. Additional 3D (H)C$_a$(C$_0$)NH, (HC$_a$)C$_\beta$(C$_a$)NH, and (HC$_a$)-C$_\beta$(C$_a$C$_0$)NH spectra were also recorded using similar parameters.[42] The U-^{13}C,^{15}N,^2H-[^{12}C,$^{13}C^2H_2$$^1H\delta$1-Ile, ^{12}C,$^{13}C^{a13}C'$,$^{13}C^2H_2$$^1H\delta$2-Leu, ^{12}C,$^{13}C^2H_2$$^1H\gamma$2-Val] sample was used. The spectra were recorded at $\omega_{0H}/2\pi = 1000$ MHz and are an excellent example of a MAS NMR version of a solution NMR HSQC and HNC$_a$ experiment and allow assignment of the ^{15}N amide resonances as well as structural measurements. Note that the peak doubling is apparent due to the presence of the two conformations in the dimer of dimers.

Measurement of Distance Restraints

Using an ILFY reverse-labeled sample, proton-assisted recoupling (PAR) MAS spectra were recorded at $\omega_{0H}/2\pi = 900$ MHz and $\omega_r/2\pi = 20$ kHz, with $\tau_{mix} = 15$ ms. The spectra, shown in Figure 5, primarily permit identification of Ca_i–Ca_{i+3} contacts. In addition, a 4-fold molar excess of rimantadine was added to the sample and had minimal impact (<0.5 ppm) on the chemical shifts, indicating that the inhibitor does not induce significant conformational changes in the S31N mutant.[18]

Proton-driven spin-diffusion (PDSD) spectra[43] were recorded at $\omega_{0H}/2\pi = 750$ MHz and $\omega_r/2\pi = 14.287$ kHz, using an ILFY reverse-labeled sample with a 4-fold molar excess of rimantadine. Primarily, C$_a$–C$_a$ contacts are shown in Figure 6. In addition, cross-peaks arising from structurally important aromatic–aromatic[18] contacts are present in the spectrum, for example, interhelical contacts from H37 Cδ2 to H37 Cδ2′ and from W41 Cη2 to W41 Cδ1′. In these spectra, we do not observe exchange between the two sets of peaks and therefore conclude that the dimer of dimers is stable on the time scale of seconds.

To establish the structure of the $M2_{18-60}$ dimer of dimers, it was important to have interhelical constraints. Accordingly, we prepared a sample with mixed ^{15}N and ^{13}C labeling and used ZF-TEDOR to detect interhelical contacts. In particular, a 1:1 mixture of U-^{15}N $M2_{18-60}$ and 1,6-^{13}C glucose-labeled $M2_{18-60}$ was refolded, ensuring that mixed tetramers were formed. ZF-TEDOR spectra were recorded at 7 μs ^{15}N π pulses, 100 kHz TPPM[44] decoupling, at $\omega_{0H}/2\pi = 800$ MHz, using $\tau_{mix} = 7.168$, 14.336, and 21.504 ms, with the optimal intensity for most cross-peaks being observed at 14.336 ms. The ZF-TEDOR experiment permitted identification of five unambiguous and one ambiguous interhelical contact shown in Figure 7.

In addition, 10 interhelical contacts (more than any other single experiment) were identified in homonuclear ^{13}C–^{13}C RFDR spectra of a ^{13}C-labeled sample prepared from 1,6-$^{13}C_2$ glucose. This produces the same labeling pattern as that in 1-^{13}C glucose[33] but with twice the site labeling level (approaching 90% incorporation). Since the ^{13}C are magnetically dilute, the deleterious effects of dipolar truncation are attenuated in measurements of weak couplings.[45] Two different spectra were recorded with broad-band RFDR using $\tau_{mix} = 8$ and 19.2 ms. In Figure 8, the cross-peaks labeled in red are interhelical and were acquired with $\tau_{mix} = 8$ ms. Also present in the spectrum are multiple inter- and intraresidue cross-peaks labeled with green and black, respectively. Two additional cross-peaks (gray) are present, which are assigned to intertetramer contacts.

The final two experimental data sets used to constrain distances were obtained from ^1H-detected 3D and 4D spectra recorded at $\omega_{0H}/2\pi = 800$ MHz that used ^1H–^1H RFDR recoupling and provided inter- and intramolecular methyl–methyl and His–Trp distances. The pulse sequence used for acquiring ^1H–^1H distances between the $^{13}C^2H_2{}^1H$–$^{13}C^2H^2{}^1H$ groups is similar to a recently reported 4D experiment using DREAM mixing[46] and to a CP-based implementation.[47] In particular, we used high spinning frequencies ($\omega_r/2\pi = 60$ kHz) and INEPT for ^{13}C–^1H and ^1H–^{13}C transfers. ^1H–^1H recoupling for the observation of long-range contacts was accomplished using RFDR ($\omega_1/2\pi = 100$ kHz) with $\tau_{mix} = 8$ ms, together with 300 ms of water suppression, as suggested by Rienstra and coworkers.[48] The timing diagram for the experiment is shown in Figure 9, and selected strips are displayed in Figure 10.

Finally, a 3D ^{15}N–^1H–^1H MAS spectrum using 3.33 ms of ^1H–^1H RFDR was recorded at $\omega_r/2\pi = 60$ kHz using 100 kHz RFDR pulses. The cross-peak intensities were identified and observed in 2D as the mixing time was varied between 0.267 and 3.33 ms. The spectrum is shown in Figure 13B and highlights the structurally important H37'-Hε2 to W41-Hε1 side chain contact in orange. Notably, the intermolecular cross-peak is more intense than similar intramolecular H37-W41 cross-peaks but less intense than 2.8 Å backbone amide contacts. This indicates a close intermolecular approach, consistent with the calculated structure, and is an essential new feature of the dimer of dimers motif.

Conversion of Peak Volumes to Distance Restraints

For ^{13}C–^{13}C restraints, peak volumes of known distances (Cα_i–Cα_{i+1} and Cα_i-Cα_{i+3}) and a distance dependence of r^{-3} were used to calibrate distance restraints. For ^{13}C–^{13}C RFDR, Cα_i–Cα_{i+1} peaks (3.8 Å distance) were used for calibration, and an upper distance limit was

entered as 1.1 times the calculated distance plus 1 Å. For nonaromatic sites, an additional 1 Å was added to account for differences in relaxation. We did not attempt to adjust the distance limits based on the site-specific degree of labeling. For ^{13}C–^{13}C PDSD and PAR, $C\alpha_i$–$C\alpha_{i+3}$ peaks (5.3 Å distance) were used for calibration, and an upper distance limit was entered as 1.12 times the calculated distance plus 1 Å. Several restraints from the $\tau_{mix} = 8$ ms PAR spectrum were adjusted manually due to consistent violations. These restraints tended to involve carbonyl resonances, for which relaxation is expected to be different from the proton-bonded carbons used for calibration.

TALOS+ Predictions

TALOS+ predictions were made using all assigned residues both with and without the use of proton chemical shifts. A higher number of good predictions were made without the proton shifts, and we therefore excluded proton shifts in the predictions. This can be rationalized based on the sensitivity of the proton chemical shift to water accessibility,[28] which is typically low in a membrane protein and perhaps the slightly altered helical geometry[49] found in membrane proteins that may not be well-represented in the TALOS+ database.

Introduction of Helical Hydrogen Bonds

Based on the TALOS + predictions, helical hydrogen bonds were entered as distance restraints for assigned residues except where the TM and AP helices meet. Distances of 2.0 ± 0.2 Å for C_i' to HN_{i+4} and 3.0 ± 0.2 Å for C_i' to N_{i+4} were entered from P25 to L43. For one pair of helices, resonances were observed for additional residues, and these restraints were therefore continued between residues 47 and 52.

Highly Ambiguous Restraints

Highly ambiguous restraints were automatically identified in the RFDR spectra of 1,6-^{13}C glucose-labeled $M2_{18–60}$ using a cutoff of 0.25 ppm, the assignment tables, and the spectrum. Cross-peaks arising from side bands or truncation artifacts were removed by manual inspection. The restraints were then filtered against a structure generated without these ambiguous restraints but including all manually entered restraints. Restraints that violated by more than 3 Å were removed. The remaining restraints were entered directly into XPLOR as highly ambiguous restraints.

Treatment of Intertetramer Contacts

Contacts that do not fit the general channel architecture (a parallel tetramer with His-37 facing inward) were excluded from the calculation and may be due to intertetramer contacts that arise due to the high concentration of protein in the membrane. For example, Val and Trp are at opposite sides of the membrane, and cross-peaks that are seen between them most likely arise from contacts between adjacent tetramers, which are inserted in an antiparallel arrangement in the membrane. This arrangement is not surprising, given the wedge shape of M2 with a large C-terminal base, and is the arrangement observed in crystal structures of TM $M2_{22–46}$.

Structure Calculations

Simulated annealing was performed using the program XPLOR-NIH.[50] Due to the C_2 symmetry, there are two different interfaces between each helix and its two neighbors. Each restraint was therefore entered as an ambiguous restraint to either of the neighboring helices. Since use of ambiguous restraints results in a rough energy landscape in which the protein is easily trapped in a local minimum, satisfying one of the possibilities, these ambiguous restraints resulted in slow convergence if introduced too early. First, TALOS+ and hydrogen-bonding restraints were introduced in a standard simulated annealing (SA) protocol, and once the structure converged, the four helices were aligned loosely by applying four-fold symmetric restraints (upper bound 6 Å) from D44Cγ–R45Cζ, H37Cε1–H37Cε1, and V27Cγ–V27Cγ. Next, noncrystallographic restraints (NCS) were turned on to ensure C_2 symmetry, and 33 structures were calculated that satisfied these modeling restraints, TALOS+, and hydrogen-bond restraints. Modeling restraints were turned off and all experimental restraints were included in the final two annealing cycles. First, 30 structures were calculated from each of the 33 structures from the previous annealing. Next, the lowest energy structure from each set of 30 structures was taken as input for calculation of an additional 30 structures. From each of these sets of 30 structures, the lowest energy structure was selected, and the lowest 20 out of 33 final structures were included in the reported ensemble. During annealing, a database-derived potential for side chain rotamers (Rama) was ramped from 0.02 to 0.2. Flat-well harmonic potentials were used, with force constants ramped from 25 to 100 kcal mol^{-1} Å^{-2} for distances (dipole couplings) and 20–100 kcal mol^{-1} rad^{-2} for TALOS-based backbone dihedral restraints. Additional force constants used in the annealing were van der Waals of 0.02–4.0 kcal mol^{-1} Å^{-2}, improper of 0.1–1.0 kcal mol^{-1} degree^{-2}, and bond angle of 0.4–1.0 kcal mol^{-1} degree^{-2}. The temperature was reduced from 1000 to 20 K in steps of 20 K and 4 ps of Verlet dynamics at each temperature with 1.5 fs time steps. The mass of all atoms was set to 100 for the annealing.

RESULTS

A set of 283 restraints consisting of 70 intrahelical distance measurements, 49 interhelical distance measurements, 72 highly ambiguous distance measurements, and 92 TALOS restraints were used to calculate an atomic resolution structure of M2$_{18-60}$ with greater than 5 restraints per residue. Interhelical restraints are depicted in Figure 11 and listed in the Supporting Information. The precision of the structure is characterized by an ensemble of twenty low-energy structures with an rmsd of 0.7 Å for backbone heavy atoms and 1.1 Å for all heavy atoms (Figure 12). The rmsd was calculated for the structured region of the protein, which extended from P25 to R45 and P25 to S50 for the two asymmetric helices, and corresponds to all consistently observed residues. Part of the amphipathic helix was observed for only one set of resonances. The residues that are not observed can be assumed to undergo microsecond to millisecond motion that interferes with the ^{1}H decoupling in MAS experiments and attenuates the intensities. This asymmetry is again consistent with the dimer of dimer structure.

The structure is packed tightly together with a narrow pore. It displays a hydrophobic surface in the direction of lipids (Figure 12) as expected for membrane proteins. At the C-

terminal base, the hydrophilic residues of the amphipathic helix are positioned to interact with the hydrophilic head groups of the lipids. In Figure 12C, the interior surface of the tetramer is drawn using the program HOLE.[51] Consistent with the understanding that the conserved residues H37 and W41 are responsible for ion selectivity and pH dependence, the narrowest part of the channel is found at these residues. The surface is colored red where less than one water molecule can fit in the channel, in green where no more than one water molecule can fit, and in blue where the pore diameter fits multiple water molecules.

Four W41 side chains are found in two distinct secondary structures (Figure 12D), with two helices in an "indole in" (W41 in Figure 13A) conformation, and the other two in an "indole out" (W41′ in Figure 13A) conformation, which in combination with the helix displacement allows the tetramer to pack into a tight bundle with a continues hydrophilic interior. Notably, the M2 channel contains very few hydrophilic residues lining the pore, particularly toward the N-terminus, where a stretch of six hydrophobic residues from P25 to A30 span nearly two helical turns. The result that adjacent helices are out of register decreases the distance between hydrophilic residues, improving the ability of the channel to form a hydrophilic pathway for proton conduction along the pore. The two-fold symmetric structure raises the possibility for an intermolecular mechanism of H^+ translocation in which the protons first bind to the more N-terminal H37 (Figure 13A) before continuing to the more C-terminal H37. Subsequently, given their proximity in the structure, an intermolecular transfer between H37′ and W41 could possibly precede proton exit on the C-terminal side of the protein (Figure 13A and Figure 15). Although this suggestion is consistent with the observed geometry, we do not at present have direct evidence for this pathway.

DISCUSSION

Drug Resistance

Despite the S31N mutation occurring near the pharmacological drug-binding site,[52,53] the precise influence of N31 on drug binding is unclear in the literature due to the substantial differences in reported structures that were solved for a variety of constructs under sample conditions that may not adequately mimic the viral membrane. There are two reported structures of the S31N mutant. The first of these was determined under conditions that did not bind drug in the pore of WT.[20] The other was solved with an inhibitor different from amantadine and rimantadine.[21] While previous structures have pointed toward either helix packing[9,20] or direct interaction[10] to explain drug resistance, the two-fold symmetric structure contains elements of both. In particular, the side chain of N31 points toward the pore in two helices and toward an adjacent helix in the other two, with neighboring N31 side chains close enough to form polar contacts. N31 is well-shielded from contact with the hydrophobic lipid membrane. In contrast, drug-bound structures of M2[9,26] show position 31 in the interface between two helices, with the side chain oriented toward the lipids. This implies that two of the helices of S31N must rotate for the molecule to adopt the drug-bound structure (see Figure 14). In S31N, the larger hydrophilic N31 side chain would disfavor this motion due to interaction with hydrophobic lipids. In addition, a direct interaction between the N31 side chain in the pore and the drug would be unfavorable. While both effects could contribute to resistance, it is unclear which is more important. The simplest explanation is

that in the drug-bound state position 31 points toward lipids which is favorable for serine but not asparagine. Thus, the new dimer of dimer structure of S31N shows the necessary rearrangement of the N31 orienting it away from the lipids. According to the structure of the rimantadine-bound chimera M2, this S31N structure clearly does not contain the adamantane binding pocket. For the design of a novel inhibitor, it may be useful to block the channel in the apo structure, without a helix rotation. The structure presented herein should find use in the search for novel inhibitors, which has recently identified several promising compounds.[25,29,30,54] As evident in Figure 12, the largest pocket in the pore that might be targeted by an inhibitor is the pharmacological binding site of adamantane-based drugs, near residue 31.

Regulation of the pH-dependent proton conduction and selectivity is determined largely by the conserved HxxxW motif, with the rate of conduction tuned by the pK_a of H37[14,15] and the unidirectional flow of protons controlled by W41.[55] Previous explanations of the unusual pK_a of H37 led to the proposal of imidazole–imidazolium dimerization in which the first two protons to enter the tetramer were shared in a low barrier hydrogen bond (LBHB).[15] An alternative explanation places H37 in a His-box conformation,[27] with water as the hydrogen-bonding partner.[14] The present structure deviates from a His-box conformation, but since it was solved at pH 7.8, above the first pK_a of this construct, and therefore does not rule out a LBHB at lower pH. If the dimerization does occur, some rearrangement of the helices would be expected in order to bring the $\delta 1$ and $\varepsilon 2$ nitrogens of adjacent H37s near enough to form a hydrogen bond (~5 Å in the structure). Alternatively, tuning of the H37 pK_a could be accomplished with favorable cation–π interactions. The two-fold symmetric structure has a network of π systems that could form favorable cation–π interactions between histadine and tryptophan, both within a helix, and between neighboring helices.

As noted above, the two-fold symmetric structure of the tetramer reveals that the side chain N–H groups of H37′ and W41 are in close proximity (Figure 13A). This feature emerged in the initial structure calculations and suggested the possibility that it could be confirmed with ^{1}H detected MAS experiments. Thus, we performed a (H)NHH$_{RFDR}$ experiment which yielded the 2D ^{1}H–^{15}N spectrum illustrated in Figure 13B which shows strong H37′–W41 cross peaks providing an N–N distance constraint of <3.5 Å. The proximity of these two residues suggests that an intermolecular proton transfer might be involved in the conduction, and a possible mechanism entailing this process is depicted in Figure 15. Initially, H37′ is protonated, and the transfer from H37′ through the channel is mediated via W41. An interesting question is then what is the function of the other two H37′s and W41′s in this mechanism. If significant structural changes occurred along with the proton release via W41 then, the other pair of intermonomer H37–W41 contacts might form. So it is possible that a proton relay might involve alternating formation of intermonomer H37–W41 complexes. However, the second pair of H37–W41′s are some distance removed and this would then average the two sets of cross peaks observed in the spectra. Clearly additional experiments are required to resolve these interesting questions.

Other Structures of M2

M2 structural models and structures have been determined under a variety of sample conditions, including both lipid bilayers, in detergent micelles, and crystallized from detergents. Among the complete tetramer structures, these investigations have either been conducted in detergents or have included a limited set of interhelical restraints, resulting in reported structures that show a high degree of conformational variability, which must be explained primarily from the difference in sample preparations. Surprisingly, none of the tetramer structures reported thus far are a dimer of dimers, as was recently observed in lipids via peak doubling,[18–20] except for a recent structure[56] based on oriented sample NMR and molecular dynamics simulations in which the deviation from four-fold symmetry was restricted to the side chain of H37.

In this oriented sample NMR structure, the helical tilt angle was determined experimentally, and a tetramer was assembled using molecular dynamics simulations. However, such orientation constraints[57] are invariant with respect to translation and rotation about the bilayer normal. Since the four-fold symmetry of the backbone is primarily broken by translation in the S31N structure in lipids, this structure is in general agreement with the previously reported oriented sample measurements of WT M2, although there may be some differences due to the mutation. This highlights the importance of measuring interhelical contacts in the determination of structure. Ideally, restraints from oriented samples would also be included in structure determinations because orientation restraints can provide long-range information that is complementary to distance measurements. However, currently, such data are not available for the S31N mutant, and we instead used an overdetermined set of distance restraints. Finally, we should mention that the possibility of a dimeric structures for various constructs of M2 has emerged from two recent MD simulations.[58,59]

CONCLUSION

We have determined the structure of the drug-resistant S31N mutant of M2 in lipid bilayers. The experimental protocol, particularly the experiments to detect interhelical distances, could represent a paradigm for structural determinations of membrane protein samples. The side chain of the mutated residue occludes the binding site of inhibitors in the n-terminal pore, explaining drug resistance. The protein was found to adopt a dimer of dimers structure, with significant deviation from two-fold symmetry, particularly for functionally important residues H37 and W41. A short distance of <3.5 Å was found between polar side chain ^{15}N of these H and W residues, suggesting that proton conduction may progress by direct transfer from histidine to tryptophan.

Supplementary Material

Refer to Web version on PubMed Central for supplementary material.

ACKNOWLEDGMENTS

REFERENCES

1. Holsinger LJ, Alams R. Virology. 1991; 183:32. [PubMed: 2053285]

2. Pinto LH, Holsinger LJ, Lamb RA. Cell. 1992; 69:517. [PubMed: 1374685]

3. Maeda T, Ohnishi S. FEBS Lett. 1980; 122:283. [PubMed: 7202720]

4. White J, Matlin K, Helenius A. J. Cell Biol. 1981; 89:674. [PubMed: 6265470]

5. Zebedee SL, Richardson CD, Lamb RA. J. Virol. 1985; 56:502. [PubMed: 3840537]

6. Lamb RA, Zebedee SL, Richardson CD. Cell. 1985; 40:627. [PubMed: 3882238]

7. Tobler K, Kelly ML, Pinto LH, Lamb RA. J. Virol. 1999; 73:9695. [PubMed: 10559278]

8. Andreas LB, Barnes AB, Corzilius B, Chou JJ, Miller EA, Caporini M, Rosay M, Griffin RG. Biochemistry. 2013; 52:2774. [PubMed: 23480101]

9. Pielak RM, Oxenoid K, Chou JJ. Structure. 2011; 19:1655. [PubMed: 22078564]

10. Stouffer AL, Acharya R, Salom D, Levine AS, Di Costanzo L, Soto CS, Tereshko V, Nanda V, Stayrook S, DeGrado WF. Nature. 2008; 451:596. [PubMed: 18235504]

11. Cady SD, Schmidt-Rohr K, Wang J, Soto CS, DeGrado WF, Hong M. Nature. 2010; 463:689. [PubMed: 20130653]

12. Cady SD, Wang J, Wu Y, DeGrado WF, Hong M. J. Am. Chem. Soc. 2011; 133:4274. [PubMed: 21381693]

13. Schnell J, Chou J. Nature. 2008; 451:591. [PubMed: 18235503]

14. Hu F, Schmidt-Rohr K, Hong M. J. Am. Chem. Soc. 2012; 134:3703. [PubMed: 21974716]

15. Hu J, Fu R, Nishimura K, Zhang L, Zhou HX, Busath DD, Vijayvergiya V, Cross TA. Proc. Natl. Acad. Sci. U. S. A. 2006; 103:6865. [PubMed: 16632600]

16. Colvin MT, Andreas LB, Chou JJ, Griffin RG. Biochemistry. 2014; 53:5987. [PubMed: 25184631]

17. Munowitz M, Bachovchin WW, Herzfeld J, Dobson CM, Griffin RG. J. Am. Chem. Soc. 1982; 104:1192.

18. Andreas LB, Eddy MT, Chou JJ, Griffin RG. J. Am. Chem. Soc. 2012; 134:7215. [PubMed: 22480220]

19. Andreas LB, Eddy MT, Pielak RM, Chou J, Griffin RG. J. Am. Chem. Soc. 2010; 132:10958. [PubMed: 20698642]

20. Can TV, Sharma M, Hung I, Gor'kov PL, Brey WW, Cross TA. J. Am. Chem. Soc. 2012; 134:9022. [PubMed: 22616841]

21. Kovacs FA, Cross TA. Biophys. J. 1997; 73:2511. [PubMed: 9370444]

22. Kovacs FA, Denny JK, Song Z, Quine JR, Cross TA. J. Mol. Biol. 2000; 295:117. [PubMed: 10623512]

23. Song ZY, Kovacs FA, Wang J, Denny JK, Shekar SC, Quine JR, Cross TA. Biophys. J. 2000; 79:767. [PubMed: 10920010]

24. Zhou H-X, Cross TA. Annu. Rev. Biophys. 2013; 42:361. [PubMed: 23451886]

25. Williams JK, Tietze D, Wang J, Wu Y, DeGrado WF, Hong M. J. Am. Chem. Soc. 2013; 135:9885. [PubMed: 23758317]

26. Pielak RM, Schnell JR, Chou JJ. Proc. Natl. Acad. Sci. U. S. A. 2009; 106:7379. [PubMed: 19383794]

27. Acharya R, Carnevale V, Fiorin G, Levine BG, Polishchuk AL, Balannik V, Samish I, Lamb RA, Pinto LH, DeGrado WF, Klein ML. Proc. Natl. Acad. Sci. U. S. A. 2010; 107:15075. [PubMed: 20689043]

28. Walsh STR, Cheng RP, Wright WW, Alonso DOV, Daggett V, Vanderkooi JM, DeGrado WF. Protein Sci. 2003; 12:520. [PubMed: 12592022]

29. Wang J, Wu Y, Ma C, Fiorin G, Pinto LH, Lamb RA, Klein ML, Degrado WF. Proc. Natl. Acad. Sci. U. S. A. 2013; 110:1315. [PubMed: 23302696]

30. Wang JZ, Ma CL, Wang J, Jo H, Canturk B, Fiorin G, Pinto LH, Lamb RA, Klein ML, DeGrado WF. J. Med. Chem. 2013; 56:2804. [PubMed: 23437766]

31. Vuister GW, Kim SJ, Wu C, Bax A. J. Am. Chem. Soc. 1994; 116:9206.

32. Atreya HS, Chary KVR. Curr. Sci. India. 2000; 79:504.

33. Lundstrom P, Teilum K, Carstensen T, Bezsonova I, Wiesner S, Hansen DF, Religa TL, Akke M, Kay LE. J. Biomol. NMR. 2007; 38:199. [PubMed: 17554498]

34. Rosen MK, Gardner KH, Willis RC, Parris WE, Pawson T, Kay LE. J. Mol. Biol. 1996; 263:627. [PubMed: 8947563]

35. Gans P, Hamelin O, Sounier R, Ayala I, Dura MA, Amero CD, Noirclerc-Savoye M, Franzetti B, Plevin MJ, Boisbouvier J. Angew. Chem., Int. Ed. 2010; 49:1958.

36. Volk J, Herrmann T, Wuthrich K. J. Biomol. NMR. 2008; 41:127. [PubMed: 18512031]

37. Barbet-Massin E, Pell AJ, Retel JS, Andreas LB, Jaudzems K, Franks WT, Nieuwkoop AJ, Hiller M, Higman V, Guerry P, Bertarello A, Knight MJ, Felletti M, Le Marchand T, Kotelovica S, Akopjana I, Tars K, Stoppini M, Bellotti V, Bolognesi M, Ricagno S, Chou JJ, Griffin RG, Oschkinat H, Lesage A, Emsley L, Herrmann T, Pintacuda G. J. Am. Chem. Soc. 2014; 136:12489. [PubMed: 25102442]

38. Jaroniec CP, Filip C, Griffin RG. J. Am. Chem. Soc. 2002; 124:10728. [PubMed: 12207528]

39. Daviso E, Eddy MT, Andreas LB, Griffin RG, Herzfeld J. J. Biomol. NMR. 2013; 55:257. [PubMed: 23334347]

40. Bennett AE, Rienstra CM, Griffiths JM, Zhen WG, Lansbury PT, Griffin RG. J. Chem. Phys. 1998; 108:9463.

41. Bennett AE, Ok JH, Griffin RG, Vega S. J. Chem. Phys. 1992; 96:8624.

42. Knight MJ, Webber AL, Pell AJ, Guerry P, Barbet-Massin E, Bertini I, Felli IC, Gonnelli L, Pierattelli R, Emsley L, Lesage A, Herrmann T, Pintacuda G. Angew. Chem., Int. Ed. 2011; 50:11697.

43. Szeverenyi NM, Sullivan MJ, Maciel GE. J. Magn. Reson. 1982; 47:462.

44. Bennett AE, Rienstra CM, Auger M, Lakshmi KV, Griffin RG. J. Chem. Phys. 1995; 103:6951.

45. Hohwy M, Rienstra CM, Jaroniec CP, Griffin RG. J. Chem. Phys. 1999; 110:7983.

46. Huber M, Hiller S, Schanda P, Ernst M, Bockmann A, Verel R, Meier BH. ChemPhysChem. 2011; 12:915. [PubMed: 21442705]

47. Linser R, Bardiaux B, Andreas LB, Hyberts SG, Morris VK, Pintacuda G, Sunde M, Kwan AH, Wagner G. J. Am. Chem. Soc. 2014; 136:11002. [PubMed: 24988008]

48. Zhou DH, Rienstra CM. J. Magn. Reson. 2008; 192:167. [PubMed: 18276175]

49. Olivella M, Deupi X, Govaerts C, Pardo L. Biophys. J. 2002; 82:3207. [PubMed: 12023245]

50. Schwieters CD, Kuszewski JJ, Tjandra N, Clore GM. J. Magn. Reson. 2003; 160:65. [PubMed: 12565051]

51. Smart OS, Goodfellow JM, Wallace BA. Biophys. J. 1993; 65:2455. [PubMed: 7508762]

52. Hay AJ, Zambon MC, Wolstenholme AJ, Skehel JJ, Smith MH. J. Antimicrob. Chemother. 1986; 18:19. [PubMed: 3793659]

53. Bright RA, Shay DK, Shu B, Cox NJ, Klimov AI. JAMA. 2006; 295:891. [PubMed: 16456087]

54. Kolocouris A, Tzitzoglaki C, Johnson FB, Zell R, Wright AK, Cross TA, Tietjen I, Fedida D, Busath DD. J. Med. Chem. 2014; 57:4629. [PubMed: 24793875]

55. Tang Y, Zaitseva F, Lamb RA, Pinto LH. J. Biol. Chem. 2002; 277:39880. [PubMed: 12183461]

56. Sharma M, Yi M, Dong H, Qin H, Peterson E, Busath DD, Zhou HX, Cross TA. Science. 2010; 330:509. [PubMed: 20966252]

57. Wu CH, Ramamoorthy A, Opella SJ. J. Magn. Reson., Ser. A. 1994; 109:270.

58. Carpenter T, Bond PJ, Khalid S, Sansom MSP. Biophys. J. 2008; 95:3790. [PubMed: 18621807]

59. Chen H, Wu Y, Voth GA. Biophys. J. 2007; 93:3470. [PubMed: 17693473]

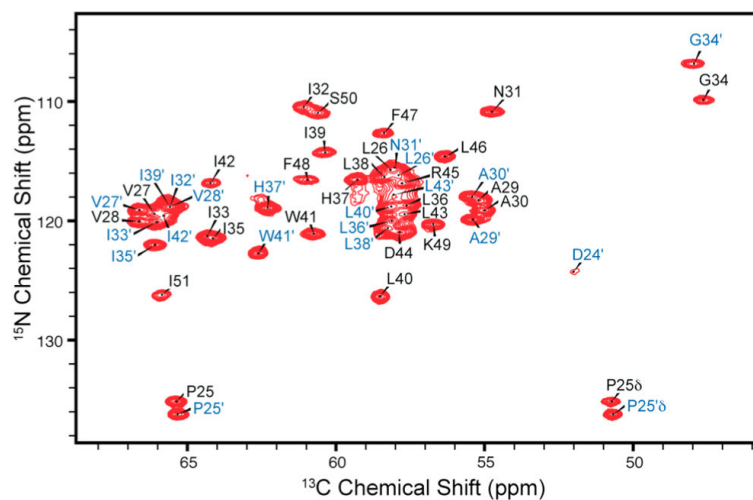**Figure 1.**
^{15}N–^{13}Cα region of the ZF-TEDOR spectrum of U-^{13}C,^{15}N S31N M2; τ_{mix} = 1.2 ms was used in order to observe only one bond transfer. Note the two sets of cross-peaks (labeled with blue and black) that correspond to the two different molecules of the M2 dimer; $\omega_{0H}/2\pi$ = 900 MHz.
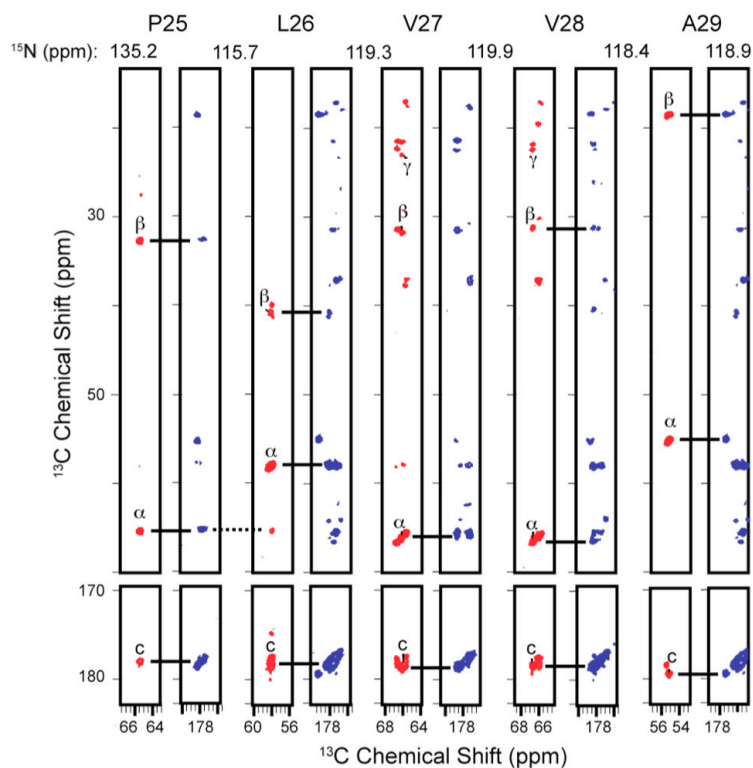
Figure 2.
Selected strips from the 3D ZF-TEDOR-RFDR spectrum recorded at $\omega_{0H}/2\pi = 900$ MHz, showing the consecutive assignment of residues P25 to A29. Mixing periods were $\tau_{mix} = 1.2$ and 4.8 ms for ZF-TEDOR and RFDR, respectively, at $\omega_r/2\pi = 20$ kHz. The NCACX transfer is shown in red and NCOCX transfer in blue.
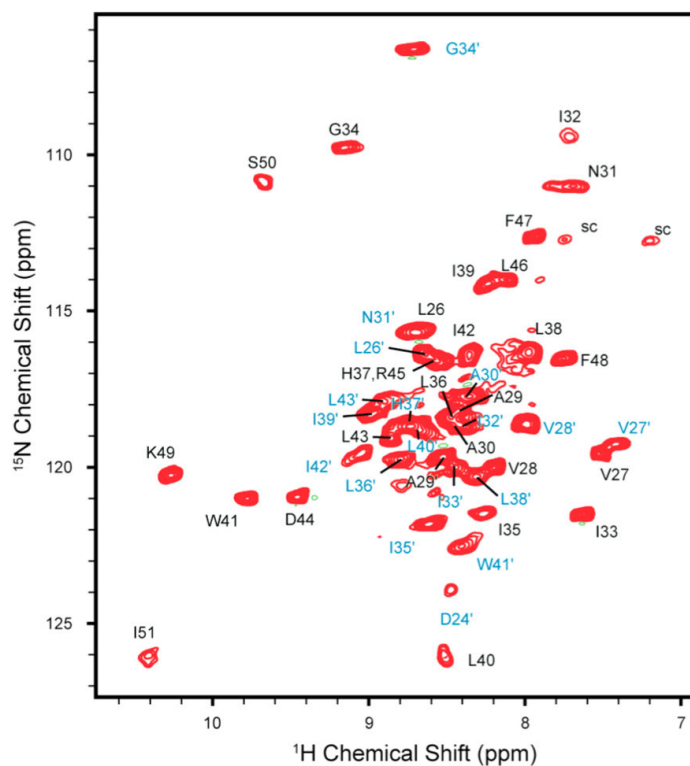
Figure 3.
Cross-polarization-based HN spectrum showing the completed backbone amide assignments for $M2_{18-60}$. Note the cross-peak doubling denoted with blue and black labels on the cross-peaks in the spectrum; $\omega_r/2\pi = 60$ kHz and $\omega_{0H}/2\pi = 1000$ MHz.
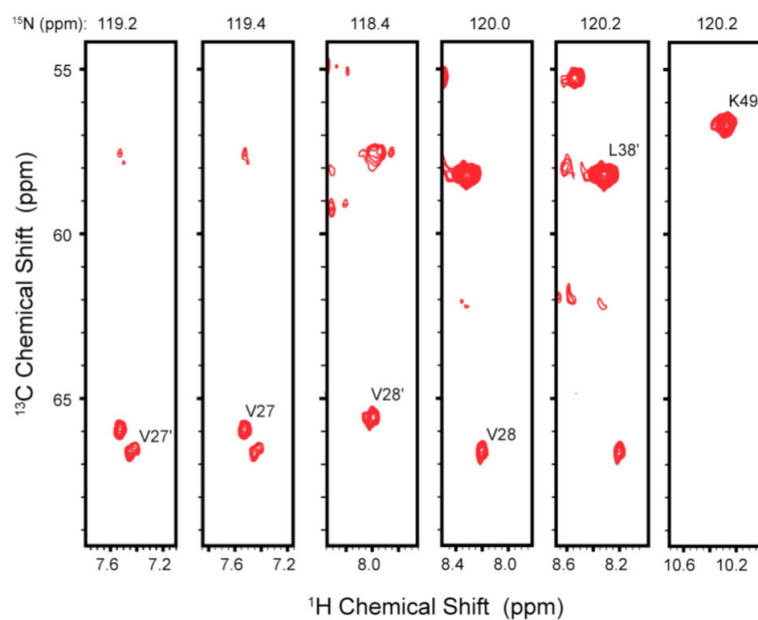
Figure 4.
Selected strips from the 3D (H)C$_\alpha$NH spectrum of ^{2}H M2$_{18-60}$ back exchanged with ^{1}H at amide sites; $\omega_{0H}/2\pi = 1000$ MHz.
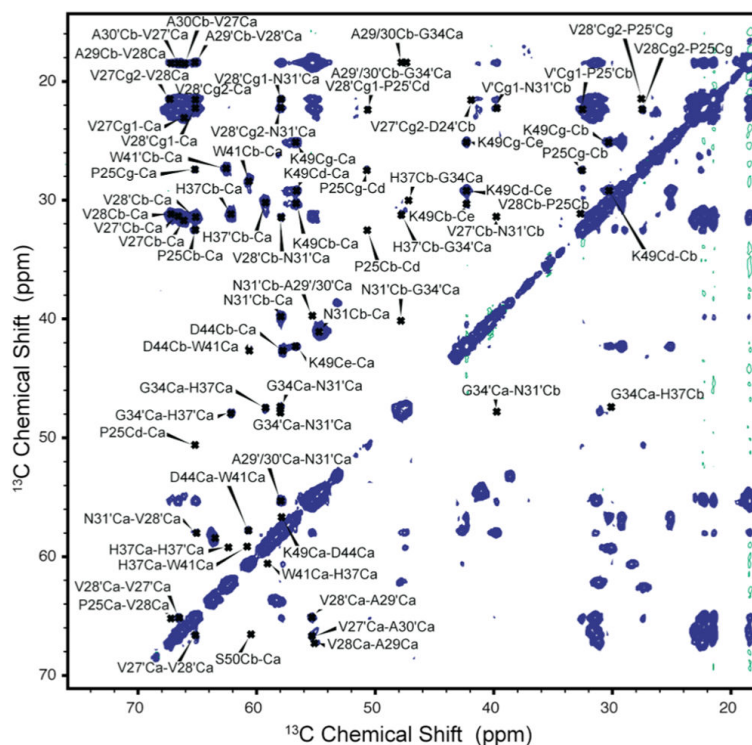
Figure 5.
^{13}C–^{13}C MAS spectrum of ILFY-labeled M2$_{18-60}$ recorded at $\omega_{0H}/2\pi = 900$ MHz and $\omega_r/2\pi = 20$ kHz using PAR mixing with $\tau_{mix} = 15$ ms. A 4-fold molar excess of rimantadine drug was present in the sample and produced minimal perturbations of the chemical shifts, as expected from an S31N M2$_{18-60}$.
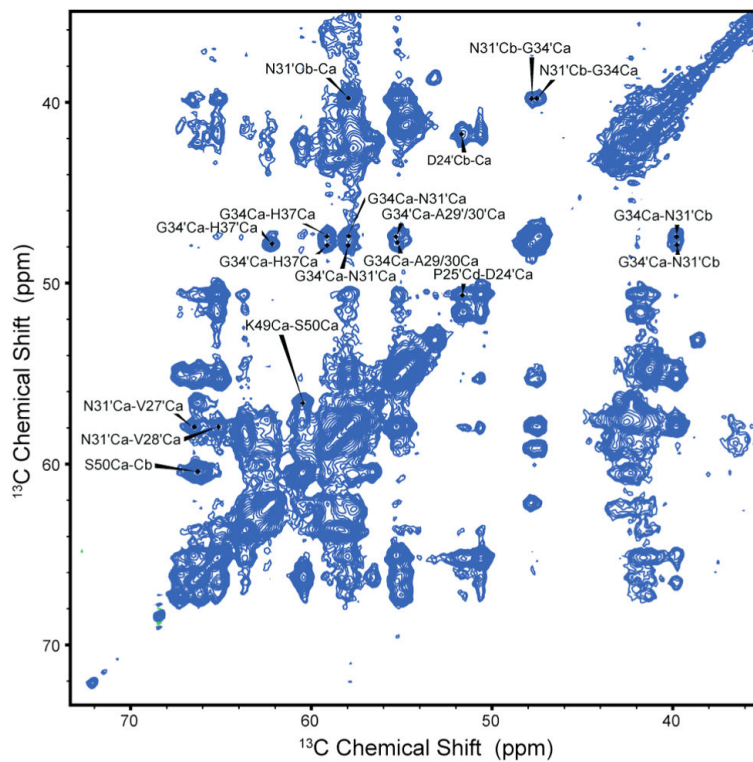
Figure 6.

C_α–C_α region of a PDSD spectrum with $\tau_{mix} = 400$ ms recorded at $\omega_{0H}/2\pi = 750$ MHz and $\omega_r/2\pi = 14.287$ kHz. A 4-fold molar excess of rimantadine drug was present in the sample and did not perturb the chemical shifts of the S31N mutant.
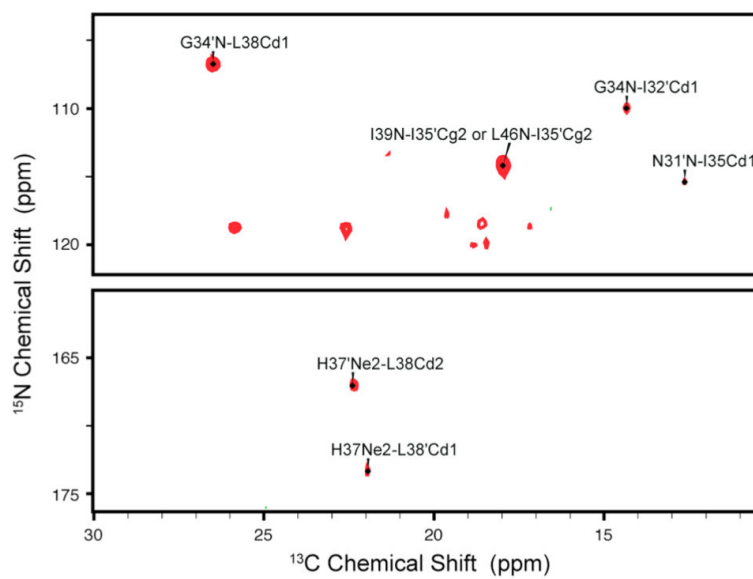
Figure 7.
^{15}N–^{13}C aliphatic correlations from a ^{15}N–^{13}C ZF-TEDOR spectrum of a 1:1 mixture of ^{15}N and 1,6-^{13}C glucose-labeled M2$_{18–60}$ recorded with τ_{mix} = 14.3 ms.
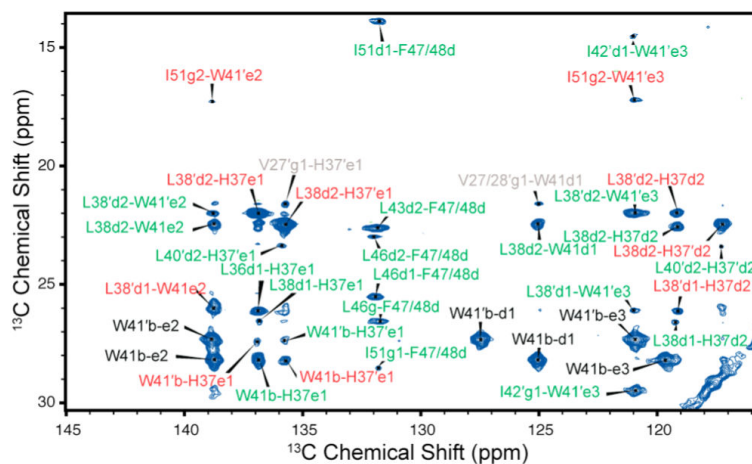
Figure 8.
^{13}C–^{13}C RFDR spectrum of 1,6-^{13}C glucose-labeled M2$_{18-60}$ showing interhelical cross-peaks (red labels) inter-residue cross-peaks (green), and intraresidue cross-peaks (black). Gray labels indicate cross-peaks that can only be explained due to the presence of intertetramer contacts. The spectrum was acquired with broad-band RFDR at $\tau_{mix} = 8$ ms, $\omega_1/2\pi = 100$ kHz of ^1H TPPM decoupling, $\omega_r/2\pi = 20$ kHz, and $\omega_{0H}/2\pi = 900$ MHz.
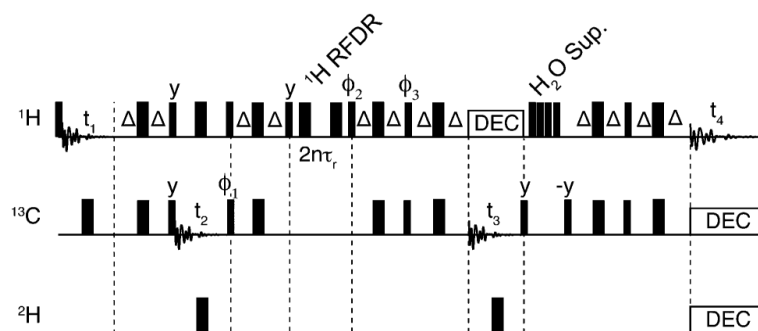
Figure 9.
Timing diagram for the 4D $^{13}C^2H_2^1H$–$^{13}C^2H_2^1H$ distance in the HCHHCH spectrum shown in Figure 10. Narrow and wide pulses represent 90 and 180° pulses, respectively. The delay was optimized for transfer via the C–H J-coupling. RFDR and H_2O suppression blocks were looped to reach the correct time. Low-power TPPM or WALTZ decoupling was used during ^1H acquisition. Phases were X unless indicated, and $\varphi_1 = 13$, $\varphi_2 = 1111\ 3333$, $\varphi_3 = 0022$, and $\varphi_{rec} = 0220\ 2002$.
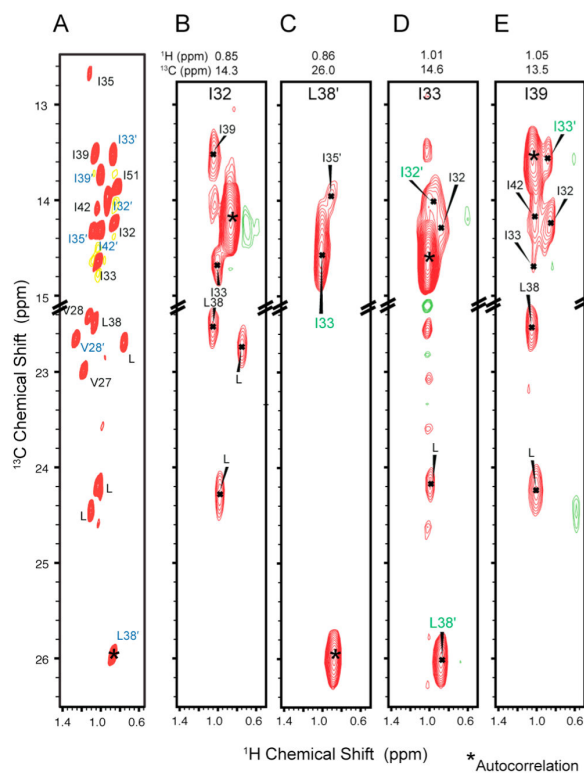
Figure 10.
Methyl spectra of M2$_{18-60}$ labeled with $^{13}C^2H_2{}^1H$ groups in the I, L, and V residues. The *J*-transferred 2D spectrum of the stereospecifically $^{13}C^2H_2{}^1H$-labeled sample is shown in A, with assignments of isoleucine Cδ1, leucine Cδ2, and valine Cγ2 methyl groups. Notice the excellent resolution and the peak doubling observed in other $^{13}C/^{15}N$ spectra. B–E show selected planes from a ^1H-detected 4D using ^1H–^1H RDFR and τ_{mix} = 8 ms and *J*-coupling-based transfers for ^{13}C–^1H correlation. Interhelical correlations are shown in green. Autocorrelations are indicated with asterisks. Details of the pulse sequence are shown in Figure 9.
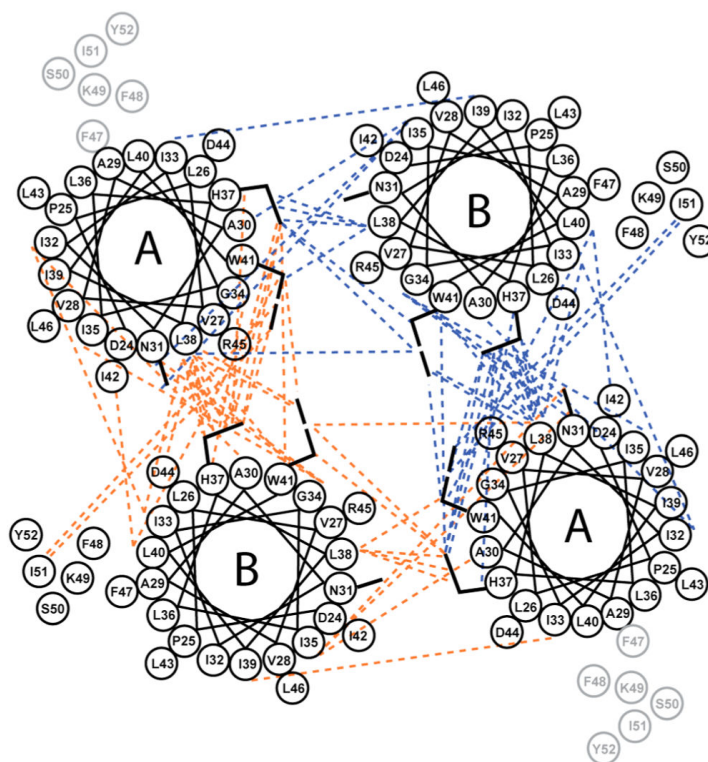
Figure 11.
Helical wheel representation of a two-fold symmetric M2 tetramer depicting the set of interhelical restraints (dashed lines) used in the final annealing, after resolution of ambiguities. The side chains of important residues N31, H37, and W41 are indicated with solid black lines.
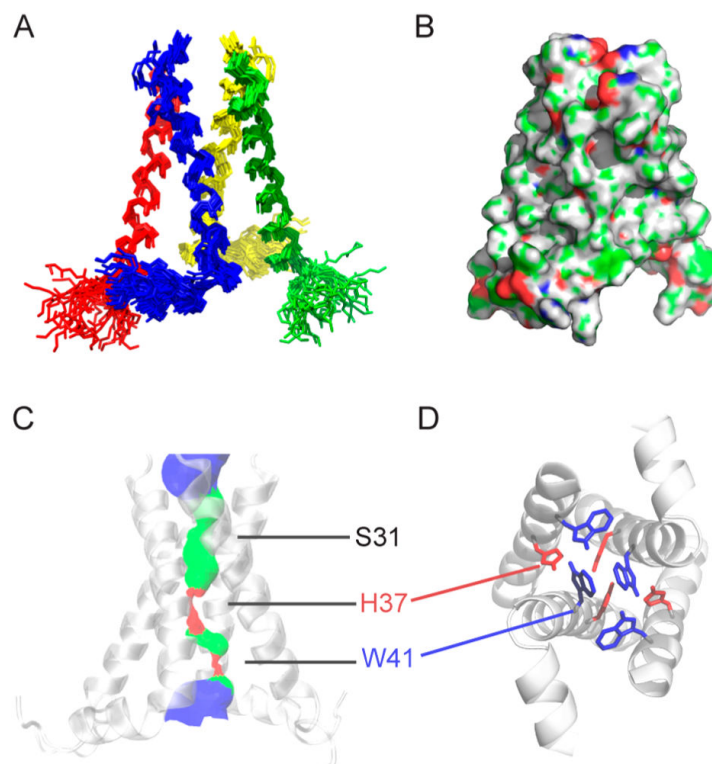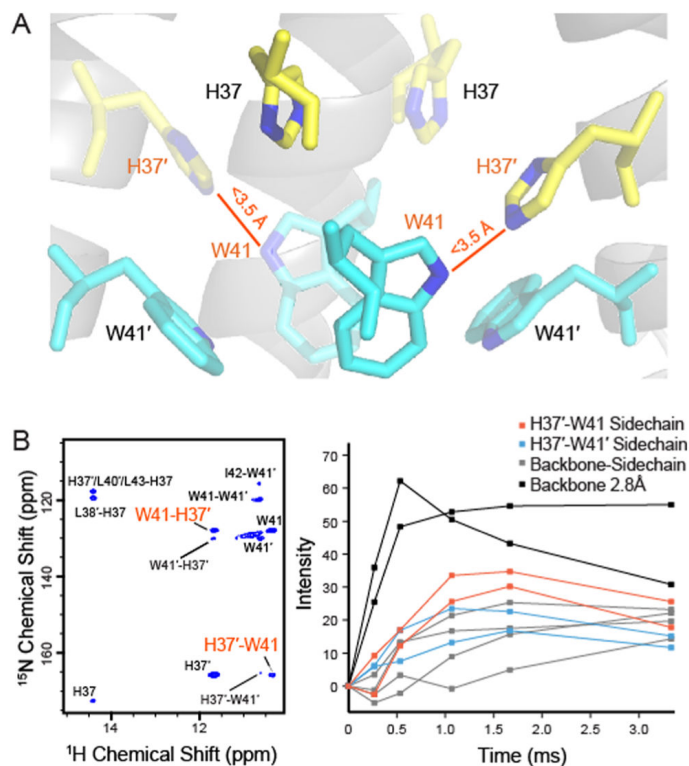
Figure 12.
Dimer of dimers structure of M2. (A) Ensemble of seven low-energy structures. The backbone and all heavy atom rmsd values are 0.7 and 1.1 Å, respectively. (B) Surface representation showing a continuous hydrophobic exterior. (C) Pore surface as calculated using the program HOLE, colored in red, green, and blue for pore widths of <1 water, 1 water, and >1 water, respectively. (D) C-terminal view of the pore with H37 in red and W41 in blue in two distinct side chain conformations. W41 adopts an "indole in" conformation for one helix and an "indole out" conformation in the other. Unstructured N- and C-terminal residues are not displayed.

Figure 13.
(A) Assembly of four H37 and W41 residues within the dimer of dimers is shown. A short intermolecular distance of 3–3.5 Å is observed between H37′ and W41 in the ensemble of calculated structures calculated from the ^{13}C–^{15}N and some of the ^{1}H detected data. (B) This proximity was subsequently confirmed by an (H)NHH$_{RFDR}$ spectrum recorded showing H37′–W41 cross peaks recorded with τ_{mix} = 3.33 ms of ^{1}H–^{1}H RFDR recoupling. The buildup of this peak is shown for a range of mixing times together with other assigned crosspeaks including a ^{1}H–^{15}N backbone distance a calibration.
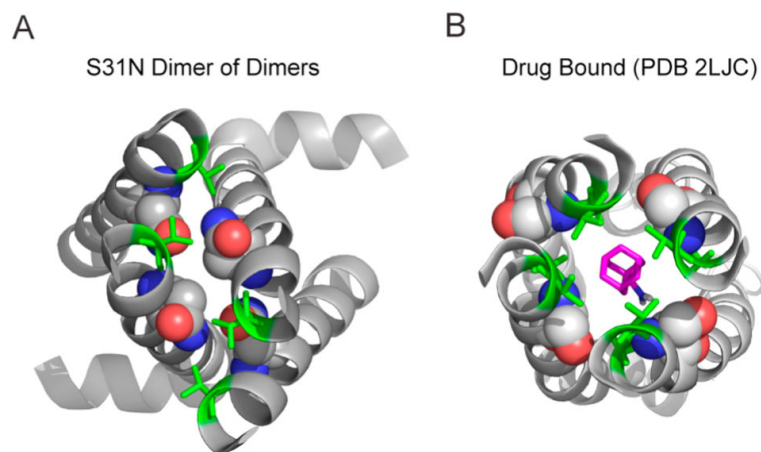
Figure 14.
S31N and drug-bound structures explain drug resistance.The S31N structure in lipids (A) places N31 in the pore or in the helix–helix interface. The WT chimera structure (B) with bound drug (pdb code 2LJC) places S31 in the helix–helix interface pointing out toward the lipid membrane mimetic. Drug is shown in magenta, the drug-binding pocket (V27 and A30) is depicted as green sticks, and residue 31 (serine or asparagine) is shown as spheres.
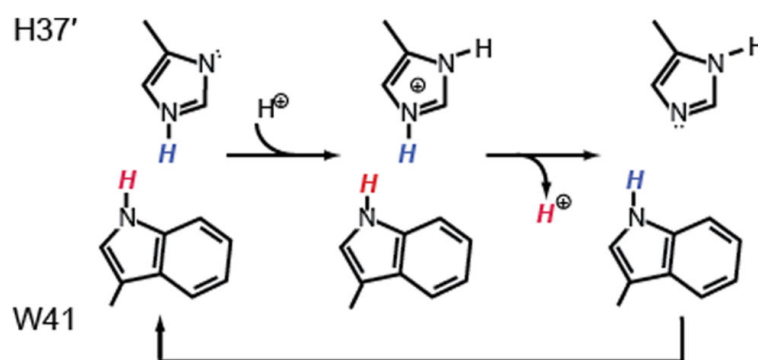
Figure 15.
A possible conduction mechanism consistent with the close proximity of H37′ and W41 found in the dimer of dimers structure (Figure 13A). The black H represents a proton that enters the channel from the n-terminal side. The blue H represents a proton transferred from H47 to W41. The red H represents the proton that can be readily released into the virus. Tautomerization of the H37 side-chain brings the protein back to the original state.